Journal of Colloid and Interface Science 537 (2019) 615–628

Contents lists available at ScienceDirect

Journal of Colloid and Interface Science

journal homepage: www.elsevier.com/locate/jcis

Regular Article

# Enzyme activation by alternating magnetic field: Importance of the bioconjugation methodology

Ilaria Armenia [a], María Valeria Grazú Bonavia [b,c,*], Laura De Matteis [d], Pavlo Ivanchenko [e], Gianmario Martra [e], Rosalba Gornati [a], Jesus M. de la Fuente [b,c], Giovanni Bernardini [a,*]

[a] Dipartimento di Biotecnologie e Scienze della Vita, Università degli Studi dell'Insubria, Via J.H. Dunant 3, 21100 Varese, Italy
[b] CIBER BBN, C Mariano Esquillor S-N, Zaragoza 50018, Spain
[c] Aragón Materials Science Institute (ICMA), Universidad de Zaragoza, CSIC, Campus Río Ebro, Edificio I+D, Mariano Esquillor Gómez, 50018 Zaragoza, Spain
[d] University of Zaragoza (UNIZAR), C Mariano Esquillor S-N, Zaragoza 50018, Spain
[e] Dipartimento di Chimica & Centro Interdipartimentale "Nanostructured Interfaces and Surfaces" – NIS, Università degli Studi di Torino, Via P. Giuria 7, 10125 Torino, Italy

## GRAPHICAL ABSTRACT

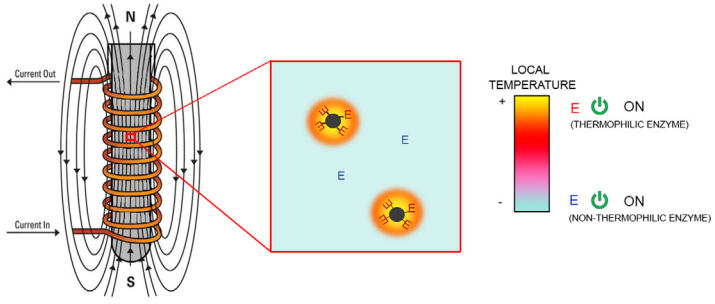


## ARTICLE INFO

*Article history:*
Received 4 September 2018
Revised 12 November 2018
Accepted 13 November 2018
Available online 14 November 2018

*Keywords:*
AMF
Magnetic nanoparticles
L-aspartate oxidase
α-Amylase
Site-directed immobilization

## ABSTRACT

Iron oxide nanoparticles (NPs) are attractive materials for enzyme immobilization and, thanks to their superparamagnetism, can be accessed by remote stimuli. This can be exploited to activate molecules that are not remotely actuable. Here, we demonstrate that thermophilic enzymes chemically linked to NPs can be activated in a "wireless" fashion by an external alternate magnetic field (AMF). To this aim, we have conjugated, with different binding strategies, the thermophilic enzymes α-amylase and L-aspartate oxidase to iron oxide NPs obtaining NP-enzyme systems with activities depending on the different orientations and stretching of the enzymes. Since enzyme activation occurs without a significant rise of the "overall" temperature of the systems, we have speculated a local NP-enzyme heating that does not immediately interest the rest of the solution that remains at relatively low temperature, low enough to allow non-thermophilic enzymes to work together with the NP-conjugated thermophilic enzymes.

Nanoactuation of thermophilic enzymes by AMF has potential applications in different fields. Indeed, multi-enzymatic processes with enzymes with different temperature optima could be carried out in the same reaction pot and thermolabile products could be efficiently produced by thermophilic enzymes without suffering for the high temperatures. Moreover, our findings represent a proof of concept of the possibility to achieve a fine-tuning of the enzyme-NP system with the aim to intervene in cell metabolism.



* Corresponding authors at: CIBER BBN, C Mariano Esquillor S-N, Zaragoza 50018, Spain (M.V. Grazú Bonavia) and DBSV, University of Insubria, Via Dunant 3, 21100 Varese, Italy (G. Bernardini).
*E-mail address:* giovanni.bernardini@uninsubria.it (G. Bernardini).

https://doi.org/10.1016/j.jcis.2018.11.058
0021-9797/

## 1. Introduction

Enzymes have higher selectivity, specificity and efficiency than chemical catalysts. Due to their properties and their green chemistry, biocatalysts are widely used in food, textile and pharmaceutical industry [1,2]. A high efficient biocatalyst for industrial applications must be stable in a wide range of temperatures and pHs and has to be easily separated and recovered from the product during the downstream process [3–5]. Enzymes present thermal instability, susceptibility to attack by protease, activity inhibition, high sensitivity to pH and other denaturing agents, and cannot be separated at the end of reaction and reused. The immobilization of enzymes on solid supports, such as polymeric resins and inorganic materials [6], overcomes these drawbacks. In this context, nanoparticles (NPs), and in particular iron oxide NPs, have been used for the conjugation of enzymes thanks to their high surface area, high surface-volume ratio, low mass transfer limitation and their unique magnetic properties [7,8]. Indeed, iron oxide NPs can be manipulated by an external magnetic field [9,10], and, as a consequence of Neel and Brown relaxation, they can produce heat under alternating magnetic field (AMF), a phenomenon known as magnetic hyperthermia [10]. This has found application in biomedicine, where its use for cancer therapy and for controlling drug delivery is being extensively explored [11–13]. However, the use of this property to improve biocatalytic processes is still almost totally unexplored.

Some authors, rather than using magnetic NPs as heat sources, have enhanced the activity of the linked enzymes by applying low frequency AMF. Magnetic energy is converted into a rotational motion of the enzyme-particle system that increase the collision rate with the substrate [14,15], or triggers conformational changes on the enzyme three-dimensional structure [16]. The use of heat generated by magnetic NPs to regulate enzyme activity has been also reported, but limited to deswelling-swelling of thermosensitive polymers attached to the NP surface that force to interact substrate-bound therapeutic drugs with enzymes that trigger their release [17–19].

The effect of the heat generated by high frequencies of AMF on enzymes directly attached to NPs has been though scarcely studied. Only Suzuki and colleagues have recently reported the specific activation of α-amylase and DNA ligase immobilized on ferromagnetic microparticles triggered by AMF [5,20]. However, this effect has not been reported yet using superparamagnetic NPs, nor it has been studied the effect of the enzyme orientation on the NP surface and of conformational changes caused by the conjugation strategy. In the case of ferromagnetic microparticles, the application of a magnetic field triggers their aggregation that cannot be easily reversed since it would be necessary to heat the particles above their Curie temperature (858°K for iron oxide) [21]. Instead, in the case of superparamagnetic NPs, magnetic properties do not persist when the external magnetic field is removed. This is an important advantage of superparamagnetic NPs over ferromagnetic ones thinking on the reuse of the nanobiocatalyst.

Here, we showed not only that it is possible to use AMF to activate thermophilic enzymes conjugated to superparamagnetic NPs, but also that the orientation of the enzyme molecule onto the NP surface is critical to maximize this effect. To this aim, we have functionalized iron oxide NPs with two enzymes of potential interest for industrial applications, i.e., α-amylase (AMY) from *Bacillus licheniformis* ($T_{opt}$ = 100 °C), and L-aspartate oxidase (LASPO) from *Solfolobus tokodaii* ($T_{opt}$ = 70 °C). We have taken into account their three-dimensional structure to conjugate them to iron oxide NPs through different native or genetically introduced residues to obtain different orientations of the enzymes. After studying the effect of the selected immobilization methodologies on the immobilization yield and activity of the bound enzyme, we carried out a physical–chemical characterization of the nano-conjugates, and applied AMF varying its frequency. We have been able to successfully activate both conjugated enzymes by the heat locally generated from the iron oxide NPs (hot-spots), without causing a significant increase in the temperature of the medium. Besides, we clearly showed that selecting an adequate immobilization methodology is a critical aspect that need to be taken into account. Indeed, the efficiency of remote enzyme activation by nanoactuation can be maximized by a specific orientation of each enzyme onto the NP surface and minimizing undesired conformational changes. Moreover, we have shown that heat remains localized around the NP-enzyme systems allowing other non-thermophilic enzymes to work together with the thermophilic ones. To this aim, we have used the non-thermophilic enzyme D-amino acid oxidase from *Rhodotorula gracilis* ($T_{opt}$ = 37 °C) in the same reaction pot of NP-AMY.

## 2. Results and discussion

### 2.1. Synthesis of aminated superparamagnetic MNPs

We have synthetized iron oxide NPs by a co-precipitation method as previously described [22] obtaining NPs with a diameter of 9.37 ± 0.5 nm (S.D.) as measured by transmission electron microscopy (Fig. 1a–d). To conjugate AMY and LASPO to iron oxide NPs, we introduced amino-groups on their surface by coating them with 3- aminopropyl triethoxysilane (APTES). We then verified that the coating of the NPs took place as expected by DLS and ζ potential analysis. DLS shows that APTES coated NPs (NP-APTES) present a hydrodynamic radius of 16.75 ± 0.5 nm (S.D.), double respect to that of uncoated iron oxide NPs (Fig. 1e). ζ potential measurements show that the superficial charge of NP-APTES is about three-fold higher than that of iron oxide NPs, i.e., 33.49 ± 0.2 mV versus 11 ± 0.8 mV. This increase in surface charge is due to the presence of the -$NH_2$ groups of APTES. To quantify the amount of primary amine groups that are present on NP surface and available for subsequent functionalization, we used the Orange II method [23,24], which is based on the electrostatic interactions between this anionic dye and the protonated amino groups in acidic solution. By means of this assay, we estimated that each NP-APTES carries an average of 22 amino groups on its surface. We also studied the colloidal stability of the NP-APTES and we did not observe any significant size change in the 3–7 pH range. Conversely, a significant loss of stability occurs at high NaCl concentration (≥100 mM) and at alkaline conditions (Supporting Information). However, this is an expected behavior as the colloidal stability provided by electrostatic repulsion is reduced at alkaline conditions due to deprotonation of the amine groups at the NP surface.

To investigate their magnetic properties, we have performed vibrating sample magnetometric analysis. The saturated magnetization value of the bare NPs was 58.7 $Am^2/kg$ $Fe_2O_3$, value that is in the range of that of the bulk material, while that of NP-APTES resulted 36.4 $Am^2/kg$ $Fe_2O_3$. This reduction can be explained by the presence of an organic coating around the particles that changes the surface magnetic anisotropy, leading to disorientation of the surface spins [25–28]. In any case, however, the magnetometry results show a superparamagnetic behavior of both NPs (Fig. 1f). We also analyzed, under an AMF of 710 kHz and 300 Gauss, the specific absorption rate (SAR) of iron oxide NPs and NP-APTES. SAR values confirm the magnetic heating ability of the NPs synthetized even after their functionalization with APTES, which generated a decrease in SAR value. Indeed, SAR is 393 ± 9 $W/g_{NP}$ for iron oxide NPs and 242 ± 13 $W/g_{NP}$ for NP-APTES.

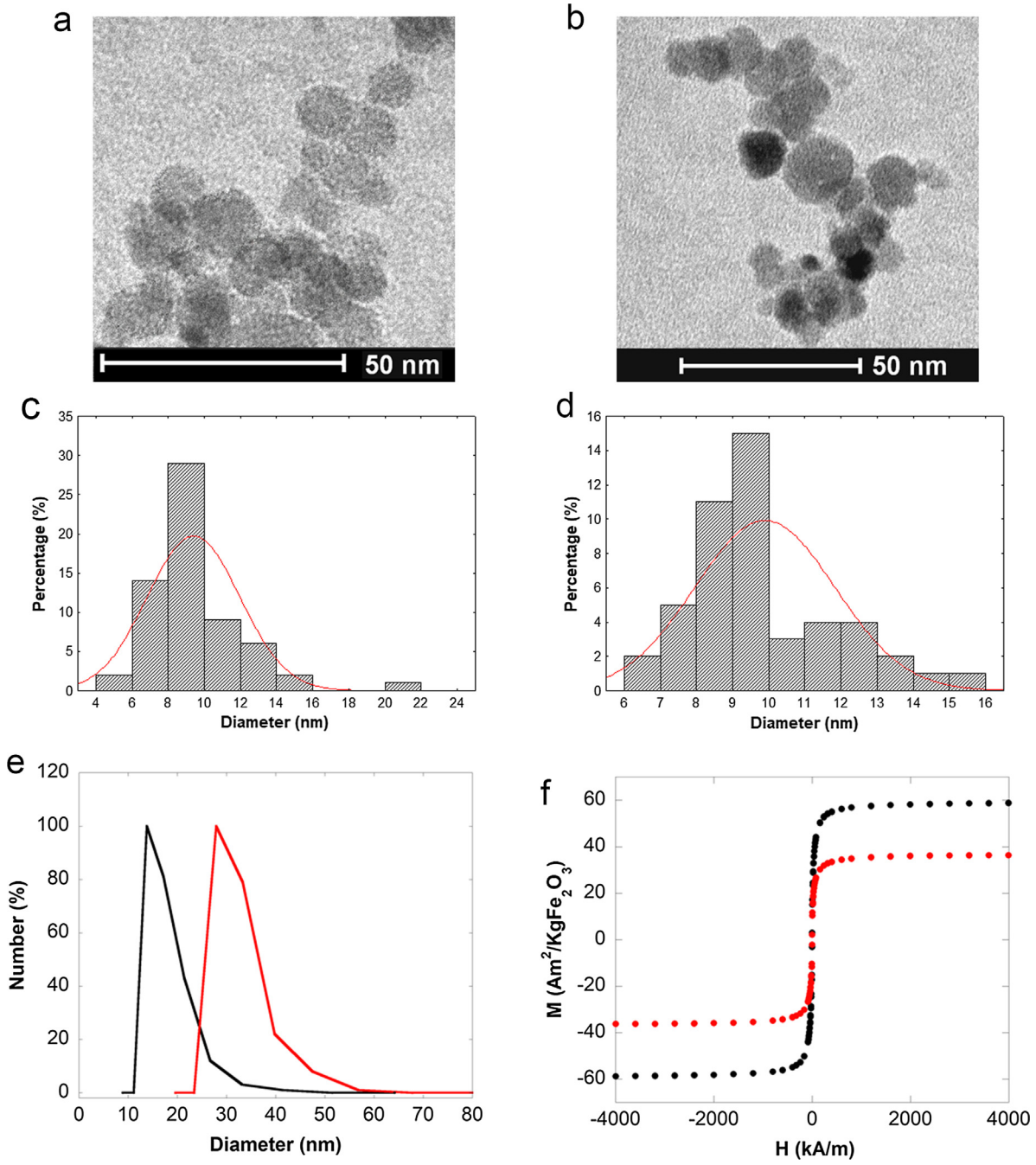


**Fig. 1.** Characterization of iron oxide NPs and NP-APTES. (a, b) TEM micrograph of iron oxide NPs and NP-APTES, scale bar 50 nm. Size distribution of iron oxide NPs (c) and NP-APTES (d). (e) DLS analysis of iron oxide NPs (Black) and NP-APTES (Red). (f) Vibrating sample magnetometry analysis of iron oxide NPs (Black) and NP-APTES (Red). (For interpretation of the references to colour in this figure legend, the reader is referred to the web version of this article.)

### *2.2. Functionalization of magnetic NPs with α-amylase and L-aspartate oxidase*

It is well known that the functionalization of the NPs with enzymes has a critical role on their activity because of deleterious conformational changes, reduction of flexibility, alteration of the hydration shell and blockage or hindering of the active site [29–31]. Therefore, with the aim to obtain different orientations of the enzyme on the NPs and to secure enzyme-NP systems with both good conjugation yield and high relative activity, we have used different conjugation strategies (Fig. 2):

***1) Strategy 1 (APTES):*** enzymes are covalently bound to the amino groups of the NPs through their carboxylated moieties after their activation with carbodiimide chemistry.

***2) Strategy 2 (APTES-Sulfo-SMCC):*** enzymes are also covalently bound via thiol groups from cysteine residues present on their surface. Before, the amino groups of the NPs need to be transformed to thiol-reactive groups by modification with sulfosuccinimidyl 4-(*N*-maleimidomethyl)cyclohexane-1-carboxylate) (Sulfo-SMCC).

***3) Strategy 3 (APTES-BS3):*** enzymes are covalently bound via their amine reactive moieties after activating the NPs amine moieties with bis(sulfosuccinimidyl)suberate (BS3).

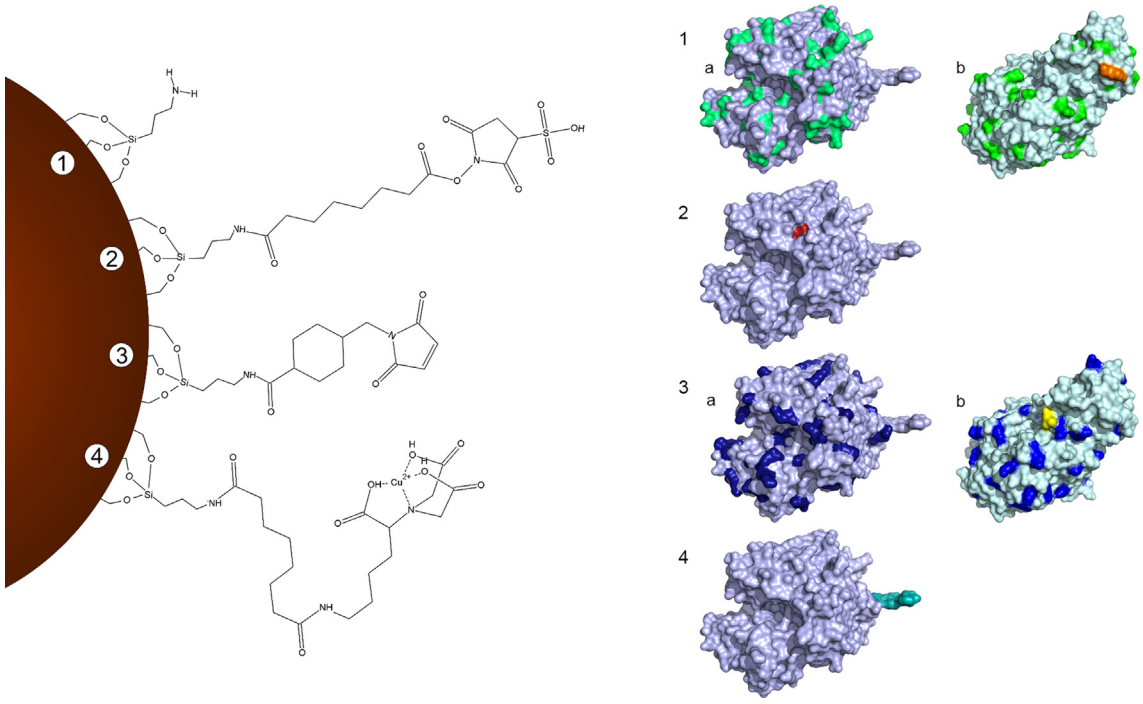


**Fig. 2.** Schematization of the expected conjugation chemistry used to link iron oxide NPs to enzyme surface. On the left, from top to bottom, we have schematized the above-described strategies: (1) APTES, (2) APTES-sulfo-SMCC, (3) APTES-BS3, and (4) APTES-NTA-$Cu^{+2}$. On the right, we reported the three-dimensional structure of the thermophilic enzymes LASPO and AMY and highlighted the residues that were available for a chemical attack. From top to bottom: carboxylic groups (strategy 1, (a) LASPO and (b) AMY), cysteine (strategy 2), amino-groups (strategy 3 a) LASPO and b) AMY) and histidine tag (strategy 4).

***4) Strategy 4 (APTES-NTA-$Cu^{+2}$):*** recombinant His-tagged enzymes are attached in an oriented way through their histidine tag by coordination with $Cu^{+2}$. The established bond, although non-covalent, is strong as hexa histidine tags show the apparent equilibrium dissociation constant in the nM range [32].

In all cases, we have evaluated the conjugation efficiency by Bradford assay, using, as a reference, the same amount of enzyme added to the NPs. Thus, changes in protein concentration in the supernatant after NP centrifugation can be correlated with the amount of the protein bound onto the NPs.

In the case of the α-amylase from *Bacillus licheniphormis* (AMY), we were able to use Strategy 1 its covalent binding to the NPs. Its crystal structure (PDB entry 1BLI) showed that while it has a large number of exposed COOH moieties, it does not present cysteine residues (needed for Strategy 2). In addition, its *N*-terminal residue was also used to its covalent binding via Strategy 3. On the other hand, Strategy 4 could not be used because the enzyme was not a His-tagged recombinant variant. AMY crystal structure also showed a homogenously distribution of COOH groups within its surface. Thus, Strategy 1 should lead to a random binding of the enzyme with respect to the orientation of its active site towards the NP surface, as depicted also by Fig. 2.

However, this conjugation strategy could also promote the formation of a covalent cross-linked enzyme@NP network depending on the pH of reaction. This as consequence of the presence on amylase's surface of primary amine groups with different pKa values from the N-terminus (pka∼7.8) and lysine residues (pka∼10.4). At pH 7.0 (NP-AMY1), only the N-terminus residue would be deprotonated and thus reactive towards the carboxylic groups of neighboring enzyme molecules activated as NHS-esters. Thus, their covalent conjugation to the most abundant amine groups of the NP surface is favored. However, at alkaline pH values (NP-AMY2), ε-amine of lysine side chain become reactive towards the activated carboxylic moieties. Thus, due to the high abundance of Lys moieties at AMY surface, the crosslinking among enzyme molecules could compete with the direct covalent binding to the NPs. Indeed, although the two conditions used to link the enzyme (pH 7 and pH 9) led to similar conjugation yields, different relative activities were obtained (61 and 36%, respectively) (Table 1).

Strategy 3 resulted in similar reaction parameters than NP-AMY1, but whit a lower relative activity. The reaction conditions promote the direct covalent binding of the enzyme via the primary amine group of its N-terminus. The reaction media pH 8.2 is slighter higher than its pKa but lower than that for ε-amine of lysine residues (∼10.5)[33] (See Table 2).

In the case of L-aspartate oxidase from *Sulfolobus tokodaii* (LASPO), we carried out the four conjugation strategies abovementioned (Fig. 2). The analysis of its crystal structure (PDB entry 2E5V), showed the presence of a high number of exposed COOH groups, which make also feasible the use of Strategy 1. However, in this case the presence of an exposed cysteine residue allowed also the use of Strategy 2. Besides, the location of this unique Cys residue ensured the site-directed attachment of the enzyme through an orientation far from its active site. Unlike AMY, this enzyme has an exposed N-terminal residue located near its active site. Thus, its binding via Strategy 3 should ensure an enzyme orientation where its active site is facing the NP's surface. Besides, as LASPO is an His-tagged recombinant enzyme, it was also possible to carry out its binding via Strategy 4. The His-tagged was added in the C-terminus of the protein that is placed opposite to the active site. Thus, this binding strategy should also render a site-directed orientation with the binding site far from the active site of the enzyme.

As reported in Table 1, the different coupling strategies led to different relative activities and number of conjugated enzyme molecules per NP. Strategy 1 was the worst one not only in terms of recovered activity after enzyme immobilization, but also in number of molecules per NP (NP-LASPO1). When the conjugation was through the exposed cysteine (Strategy 2), the best relative activity and the highest number of molecules per NP was obtained

**Table 1**
Enzyme-NPs conjugated reaction parameters.

| | Cross linker | $\mu g_{enzyme}/mg_{NPs}$ | Relative Activity (%)* | Active enzyme molecules/NP |
|---|---|---|---|---|
| NP-AMY1 | EDC NHS pH 7 | 22.5 | 61 | 3 |
| NP-AMY2 | EDC NHS pH 9 | 22 | 36 | 3 |
| NP-AMY3 | BS3 | 23 | 54 | 3 |
| NP-LASPO1 | EDC NHS pH 8.5 | 7 | 17 | 5 |
| NP-LASPO2 | Sulfo-SMCC | 25 | 87 | 22 |
| NP-LASPO3 | $BS^3$ | 37 | 86 | 17 |
| NP-LASPO4 | $NTACu^{2+}$ | 6 | 25 | 2 |

* Relative activity is the ratio between the activity assayed for the enzyme-conjugated NPs and the activity of the free enzyme.

**Table 2**
Physical parameters of the different enzyme-NP systems.

| | NP-APTES | NP-AMY1 | NP-AMY2 | NP-AMY3 | NP-LASPO1 | NP-LASPO2 | NP-LASPO3 | NP-LASPO4 |
|---|---|---|---|---|---|---|---|---|
| radius [nm] (TEM) | 4.7 ± 0.5 | 6.1 ± 0.6 | 6.25 ± 0.8 | 6.2 ± 0.5 | 5.2 ± 0.5 | 4.9 ± 1.2 | 4.9 ± 1.4 | 5.6 ± 1.3 |
| Diameter [nm] (DLS) | 46.6 ± 0.4 | 392 ± 0.6 | 873.3 ± 0.3 | 197.7 ± 0.4 | 84.4 ± 0.2 | 341 ± 0.8 | 220 ± 0.4 | 930 ± 0.4 |
| Polydispersity Index (DLS) | 0.127 | 0.185 | 0.321 | 0.191 | 0.319 | 0.2 | 0.212 | 0.301 |
| ζ-potential [mV] | 33.5 ± 0.8 | −9.04 ± 0.7 | −38. ± 0.676 | −19.04 ± 0.8 | −22.9 ± 0.5 | −32.6 ± 1.2 | −16,45 ± 0.5 | −15.88 ± 0.2 |

(NP-LASPO2). We confirmed that the binding occurred through the cysteine moiety, since the conjugation was possible only when the protein was previously reduced with TCPE reducing gel. Besides, we have checked the reversibility of the disulphide bond reducing it with DTT. This caused the complete release of the enzyme confirming the covalent nature of the functionalization (See Supporting Information). We have also obtained a high relative activity and a high number of molecules per NP using Strategy 3 (NP-LASPO3). In this case, we have set the immobilization conditions in order to promote the direct covalent binding of the enzyme via the primary amine group at its N-terminus. Thus, a pH of reaction was used slighter higher (pH 8.2) than its pKa but lower than that for ε-amine of lysine residues. However, at this pH value the enzyme has net negative charge (pI 6.75) while BS3-activated NPs have a net positive one. Thus, we cannot ensure the direct covalent binding via the enzyme amino terminus, as ionic adsorption reactions are much faster than covalent ones. Indeed, we observed ionic adsorption when we used, as a control, aminated-NPs (NP-APTES) without BS3 activation. To avoid this ionic adsorption, we used higher ionic strengths during enzyme immobilization. As this strategy did not work, we also tried to diminish the net positive charge of the NPs by carrying out the partial modification of its amino groups with an aminated-750 Da polyethylene glycol (PEG) [34,35] after their activation with BS3. However, the decrement in the net surface charge of the PEGylated-NPs was not enough to avoid LASPO ionic adsorption (See Supporting Information).

However, if we study the 3D structure of LASPO in more detail, it is possible to observe that the region with the highest amount of negative charges (COOH groups) is the enzyme area around its active site where the N-terminal is also located. Since the zone of a protein with the greater number of charged residues would have the faster ionic adsorption rate, a two-step oriented covalent binding should be taking place [36]. First, an initial rapid ionic adsorption of LASPO through this front plane of interaction occurred followed by a much slower site-directed covalent attachment via reaction of amino-groups facing the NP surface with its BS3 activated aminated groups. Although we cannot ensure a direct binding via its amino-terminal group, the final enzyme orientation obtained should be similar in both cases (See Supporting Information).

Finally, we also bind the enzyme by chelation of its histidine tag (Strategy 4), to obtain an orientation of the enzyme with its active site completely exposed to the reaction media. Although, the orientation obtained should be similar to Strategy 3, this strategy has the advantage that it is not necessary to previously modify the enzyme. The oriented binding through its His-tag was confirmed as no immobilization was observed when imidazole was included in the binding buffer. However, with this binding strategy we have obtained the worst results (NP-LASPO4) in terms of relative activity and enzyme molecules per NP. These results confirm that the activity of the NP-enzyme systems strongly depends on the chemistry of conjugation that can cause conformational changes of the enzyme or lead to non-specific bindings with the NPs [37–39].

The functionalization protocol was also followed by DLS and ζ potential measurements. Negative ζ potential values of the enzyme functionalized NPs is expected as LASPO has a net negative charge at the pH value of the measurements. With all the conjugation strategies, a partial aggregation of the NPs was observed, although NP-LASPO4 was the one showing more aggregation. This could be explained in this case by the fact that the functionalization of the NP surface to ensure the enzyme binding reduce the net charge of the particles decreasing their colloidal stability.

We have further characterized the NP-enzyme systems studying the effect of the temperature on their enzymatic activity (Fig. 3). The optimal temperature of NP-AMY1 remained that of the free enzyme, i.e., 90 °C, that of NP-AMY2 shifted to 70 °C, and that of the NP-AMY3 to 80 °C (Fig. 3a). Also, the different NP-LASPO systems have different optimal temperatures (Fig. 3b). NP-LASPO1, NP-LASPO2 and NP-LASPO3 have their optimal temperature at 70 °C (Fig. 3b; black, green and blue curves) that is similar to that of the free LASPO, while the optimal temperature of NP-LASPO4 resulted shifted to 50 °C (Fig. 3b, red curve). Again, these results confirm that the different conjugation strategies could have a different effect on the thermostability of the immobilized enzyme. In the case of NP-AMY2 and NP-LASPO4, we observed a clear lower thermal stability with respect to the free enzyme.

### 2.3. Remote enzyme activation by AMF nanoactuation

To evaluate the possibility to activate the immobilized enzymes solely by an AMF without heating the medium in which they are suspended, we have applied a 252 Gauss AMF to the different NP-enzyme systems obtained. The volume fraction of the NPs is very low and, thus we can consider them thermally isolated from each other. Consequently, no appreciable increase in the global temperature of the reaction media is expected.

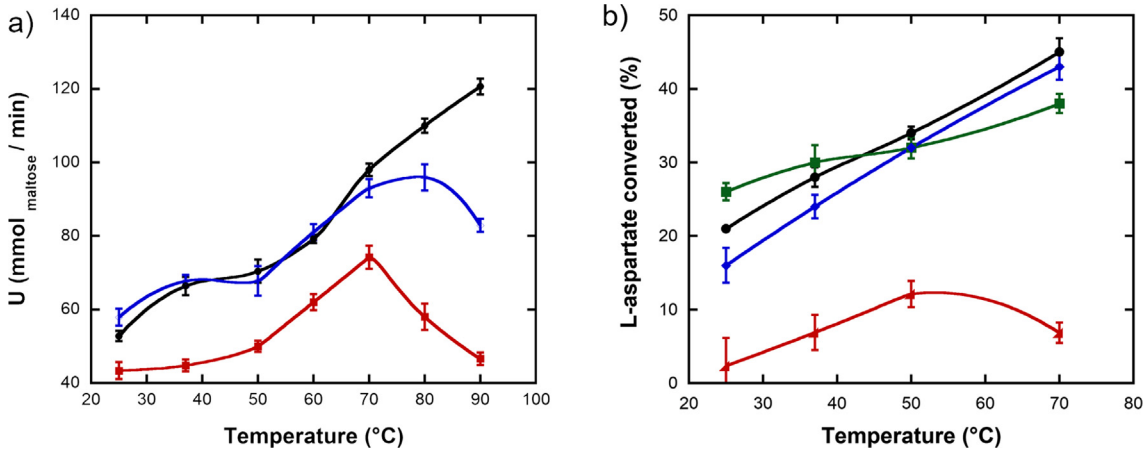


**Fig. 3.** Effect of temperature on the activity of enzyme conjugated NPs after 30 min of incubation. The activities of AMY1 (black) NP-AMY2 (red) and NP-AMY3 (blue) are compared in (a), while the activities of NP-LASPO 1 (black) NP-LASPO 2 (green), NP-LASPO 3 (blue) and NP-LASPO 4 (red) are compared in b. (For interpretation of the references to colour in this figure legend, the reader is referred to the web version of this article.)

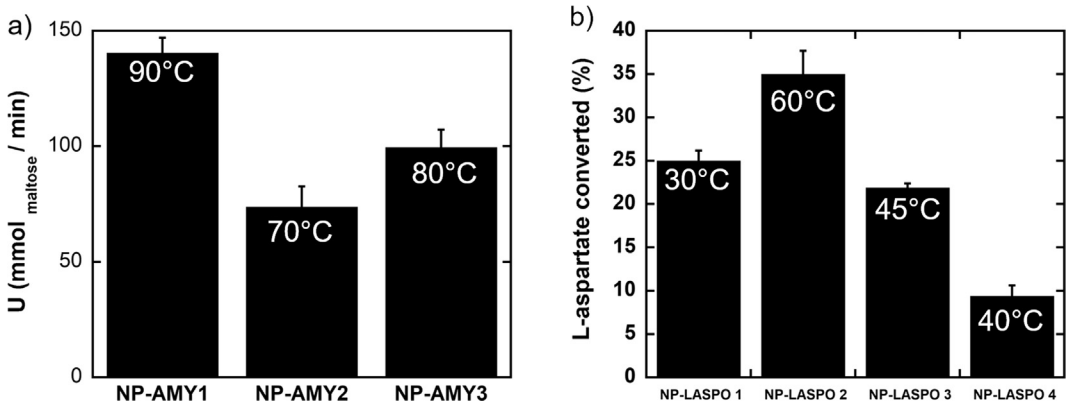


**Fig. 4.** Activity of conjugated thermophilic enzymes under a 252 Gauss AMF with a frequency of 829 KHz and after 30 min for NP-AMY1, NP-AMY2 and NP-AMY3 (a) and for LASPO1, LASPO2, LASPO3, LASPO4 (b). In the figure, we have associated to the bars, which represent the enzymatic activity obtained applying AMF, the temperatures at which the enzyme works with the same activity in the thermoblock.

As shown in Fig. 4, by applying an AMF at a frequency of 829 kHz, we have been able to remotely activate AMY and LASPO. To assess this, we compared the values of the enzymatic activity detected after exposure to the AMF to those obtained heating the sample during the same length of time, but using conventional thermal energy transfer (i.e., incubating test tubes in a thermoblock). After 30 min of exposure to AMF, NP-AMY1, NP-AMY2 and NP-AMY3 produced 140, 74 and 99 μmol × min of maltose, respectively (Fig. 4a). These activities obtained with AMF are comparable to those that can be obtained heating the sample for 30 min in a thermoblock at 90 °C for NP-AMY1, at 70 °C for NP-AMY2 and 80 °C for NP-AMY3. NP-LASPO1, NP-LASPO2 and NP-LASPO3, when exposed to an AMF, show an activity that corresponds to that obtained incubating the NP-enzyme systems in a thermoblock at 30 °C, 60 °C and 45 °C, respectively. Since the curve of the activity of NP-LASPO4 is not monotonic (Fig. 3b), for this NP-enzyme system, we cannot discriminate if the activity is comparable to the one obtained at 40 °C or at 60 °C. As the global temperature in all cases was 21 °C, the obtained results clearly showed that it was possible to activate both enzymes by AMF application whatever conjugation strategy was used. Besides, it was observed an increase of enzyme activity when increasing the frequency of the applied AMF. The higher the frequency of the applied field, the higher the increase of heat generated by the NPs, which resulted in turn in a higher activation of the immobilized enzyme (Fig. 5).

However, the efficiency of this activation depended on the coupling strategy, being the best options NP-AMY1 (Strategy 1) for the amylase. In the case of NP-AMY2 and NP-AMY3 the low activation efficiency observed could be a consequence of the thermal enzyme destabilization caused by both immobilization strategies. However, we cannot exclude a contribution due to the observed NPs aggregation triggered by enzyme binding, as it is well known that the heating efficiency of NPs drastically decreases after aggregation. In all the conditions considered, the application of the magnetic field and the subsequent activation of the thermophilic enzyme immobilized on them, did not cause an increase in the temperature of the reaction media. This can be explained by the fact that the amount of NPs used were thermally isolated due to the low concentration used.

To confirm that the reaction media temperature does not increase during the application of the AMF of 829 kHz and 252 Gauss, a reaction containing the NP-AMY preparations and the thermolable enzyme D-aminoacid oxidase (DAAO) was carried on. Table 3 reports the activity register for the two enzyme used.

It is possible to observe that the enzymes are both active: NP-AMY was activated as it is at 90°, 70 °C and 80 °C for NP-AMY1, NP-AMY2 and NP-AMY3 respectively. While DAAO shows an enzymatic activity comparable of the one obtained when the reaction is carried on at room temperature. These data prove that the application of a magnetic field in presence of NPs does not cause an excess of heating in the reaction media. Thus, it will be possible to carry

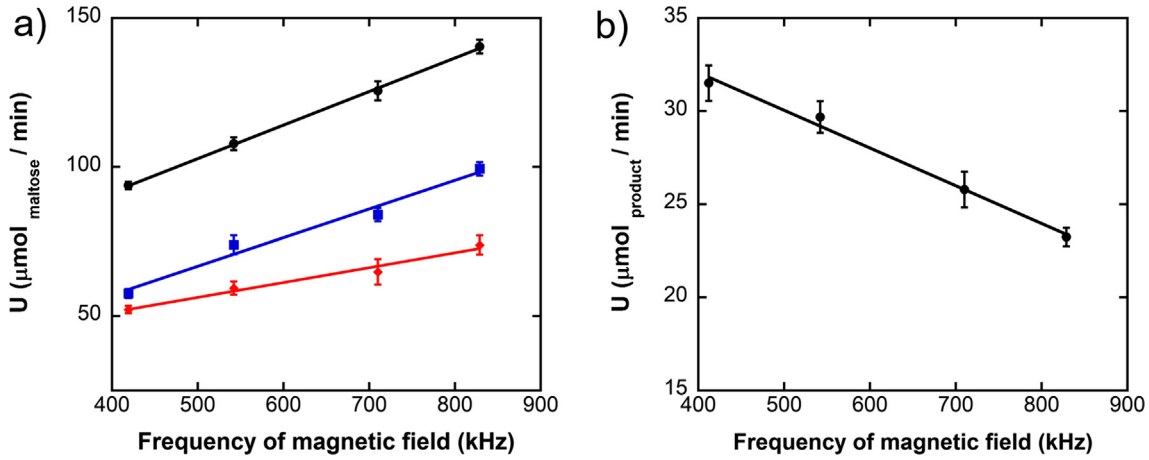


**Fig. 5.** Dependence of the enzymatic activity on AMF frequency. (a) NP-AMY 1 (black), NP-AMY 2 (red) and NP-AMY3 (blue) exposed to a 252 Gauss AMF with frequencies ranging from 410 to 829 kHz. (b) NP-DAAO exposed to a 252 Gauss AMF with frequencies ranging from 410 to 829 kHz. (For interpretation of the references to colour in this figure legend, the reader is referred to the web version of this article.)

**Table 3**
Activity of conjugated amylase and of the free DAAO under an AMF of 829 kHz and 252 Gauss.

| | U ($\mu g_{maltose} \times mg_{NP}$) | U ($\mu g_{substate} \times mg_{enzyme}$) |
|---|---|---|
| NP-AMY1/DAAO | 115 ± 0.5 | 33 ± 0.2 |
| NP-AMY2/DAAO | 75 ± 0.7 | 33 ± 0.3 |
| NP-AMY3/DAAO | 98 ± 0.4 | 33 ± 0.8 |

on multi-enzymatic processes of biotechnological interest in which one of enzyme/substrate/product is thermolable, while the other needs an high temperature to work.

As further proof of the heating transfer from the NPs to the enzyme, the DAAO was immobilized on NP-APTES as previously reported [22]. Then an AMF field of 252 Gauss and frequencies varied from 410 to 829 kHz was applied in presence of NP-DAAO and free amylase (Fig. 5).

Fig. 5 depicts that as the frequency of the AMF gets higher, the enzyme activity became lower, as the enzyme was incubated in increasing reaction temperature. DAAO is indeed a thermolabile enzyme with an optimum temperature of 37 °C that becomes partially denatured when the temperature increase. On the other hand, the free amylase, present in the reaction media, registered an activity comparable to those obtained incubating the enzyme at room temperature (data not shown).

But how to explain the large differences observed in enzyme activation efficiency among the different bioconjugation strategies? In the case of NP-AMY2 and NP-LASPO4, the low activation efficiency observed in both cases could be a consequence of the thermal enzyme destabilization caused by both immobilization strategies with respect to the free enzyme. Moreover, in the case of NP-AMY3 also the aggregation of enzymes molecules linked to the NP surface (see below) might have played a role. However, we cannot exclude a contribution due to the observed NPs aggregation triggered by enzyme binding, as it is well known that the heating efficiency of NPs drastically decreases after aggregation [40]. When we compared the activation efficiency in the case of NP-LASPO2 and NP-LASPO3, there are not significant differences between both enzyme-NPs preparations in terms of mean diameter after NPs functionalization, number of enzyme molecules per NP or their relative activity after immobilization. Besides, the optimal temperatures of both immobilized enzyme preparations were similar to the free enzyme when heated using conventional thermal energy transfer systems (thermoblock). However, the enzyme activation efficiency was clearly better in the case of NP-LASPO2 when NPs were exposed to AMF. A clear difference between both preparations could be explained by a different orientation of the enzyme once attached to the NP surface. In the case of NP-LASPO 2, the active site is located far away from the NP surface while the opposite occurs in the case of NP-LASPO 3. Thus, it seems that orientation of the enzyme once attached to the NP surface could also play a critical role in the efficiency of the enzyme activation triggered by AMF. This should be a consequence of a different mechanism of thermal energy transference and inherent different rigidities of the zones through which the enzyme is attached to the support. Checking the 3D structure of LASPO, its back-region where attachment took place when using Strategy 2 is much more rigid than the region near the active site used for the attachment in Strategy 3. This last zone has to be intrinsically more flexible to allow the conformational changes that are triggered by the presence of the enzyme substrate. The higher the rigidity of an enzyme area, the less is the susceptibility to its denaturation when exposed to a denaturant agent (co-solvents, temperature, etc.).

### 2.4. Spectroscopic characterization of α-amylase

Although the hypothesis that the orientation might influence the final activity of the enzyme-NP system appears to be sound, we think that other factors can participate to activity modification. The formation of the chemical bound that links the enzyme to the NP, indeed, could be also responsible for the stretching of the 3D conformation of the protein that in turn could alter some functional characteristic of the enzyme. To test this hypothesis, we have investigated by spectroscopic methods NP-AMY systems and compared them with the pristine enzyme. Absorption and scattering of UV–Vis light by iron oxide NPs prevented the possibility to use CD-UV spectroscopy for studying the structure of enzymes conjugated to NPs (Fig. S5 in Supporting Information). Thus, we have used IR-ATR spectroscopy, exploiting a lab-setup method allowing for the collection of IR spectra of samples kept in an aqueous environment, namely $D_2O$ (see Materials and Methods section). In infrared spectra of proteins, most of the structural information is provided by the features of amide I band (mainly due to the $\nu$C=O mode of peptide units) [41], which usually consists of a number of components heavily overlapped among each other. A curve-fitting approach must then be exploited, but it does not always lead to unequivocal solutions [42]. To increase the affordability of the IR data analysis, we have adopted the following strategy: (i) collection and analysis of the CD-UV spectrum of AMY

in $D_2O$; (ii) collection the IR-ATR spectrum of AMY in $D_2O$ and related analysis taking into account the CD-UV result; (iii) collection of IR-ATR spectra of NP-AMY1, NP-AMY2, and NP-AMY3 in $D_2O$ and subsequent analysis using as input the fitting components resulting from steps (ii).

Fig. 6 shows the CD-UV spectrum of AMY in $D_2O$, characterized by a positive signal at 190 nm and three negative signals at 209, 219, and 225 nm, in agreement with literature data [43]. The spectrum was deconvoluted (CDNN software) and the relative amount of α-helix, β-sheet, β-loops, and unordered secondary motifs are reported in Table 4, entry 1, appearing consistent with the results by Kikani and Singh [44].

Also, the IR spectrum of AMY in $D_2O$ (Fig. 7, a) appeared in full agreement with literature data [45], showing an amide I multi-subbands profile (1700–1620 $cm^{-1}$), the amide II signal located in the 1500–1400 $cm^{-1}$ range because of the N-H/N-D isotopic exchange, and minor features in the 1620–1500 $cm^{-1}$ region due to side chains amino acids (in particular, the weak band at 1515 is typical of tyrosine) [34].

The low number of enzyme molecules per NP resulted in a very weak IR pattern for NP-AMY1, NP-AMY2, and NP-AMY3 (Fig. 7, curves b-d, in the order), however a downshift accompanied by a change in shape of the amide I band was clearly observed, more extended in the case of NP-AMY3.

In the four cases, the amide I profile was properly fitted by considering five components, with maxima at 1680/1681, 1662/1663, 1650/1651, 1635/1637 and 1621/1625 $cm^{-1}$ (Fig. 8). The two components extremities of the series can be assigned to the high and low frequency signals of β-sheets, splitted by transition dipole coupling, and the others to β-turns, α-helix and unordered secondary structure motifs, in the order [42]. For AMY, the result of the fitting was fully consistent with the relative amount of secondary structure motifs obtained by CD-UV (Table 4, entries 1 and 2). By comparison, the fitting of the amide I band in the IR spectra of NP-AMY1, NP-AMY2, and NP-AMY3 (Table 4, entries 3–5, in the order) indicated that, in all cases, conjugation of AMY to NP resulted in an increase of unordered portions at the expenses of β-turns motifs, and, for NP-AMY2 and NP-AMY3, of α-helix portions. Moreover, the IR pattern of NP-AMY3 indicated the occurrence of a significant increase of β-sheet like structures, likely resulting from enzyme-enzyme interactions [46]. This feature suggests that the bioconjugation conditions adopted for preparing this system finally resulted in aggregates of AMY molecules at the NP surface.

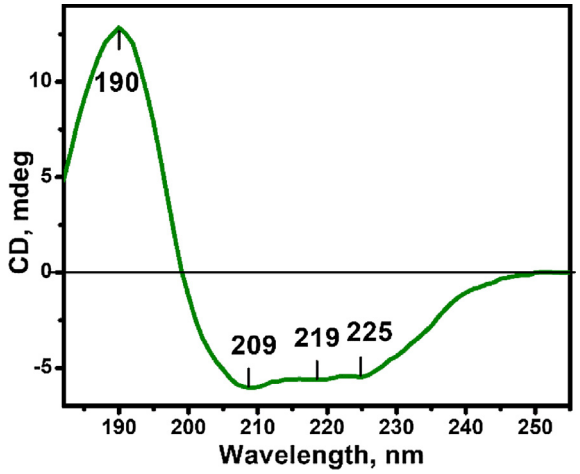


**Fig. 6.** CD-UV spectrum of a 0.07 mg/mL solution of AMY in $D_2O$.

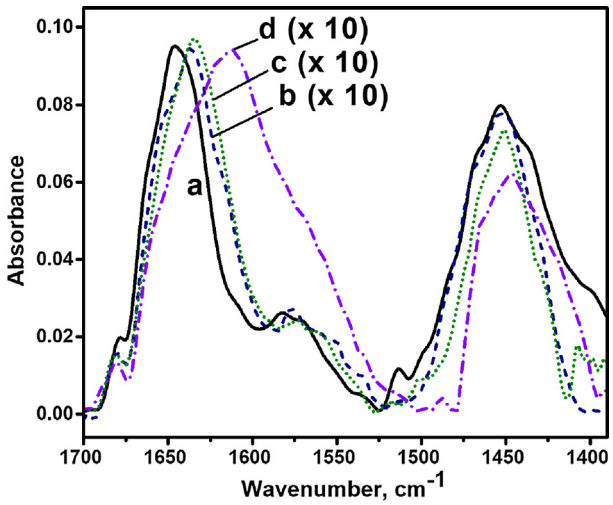


**Fig. 7.** IR-ATR spectra: (a) AMY solution ($D_2O$, ca. 20 mg/mL) collected with a horizontal-ATR cell; (b), (c), and (d) NP-AMY1, NP-AMY2, and NP-AMY3 (respectively, collected with samples in the form of a slurry in $D_2O$ pressed on the diamond internal reflection element of single-reflection ATR cell. The intensity of curves (b) and (c) are multiplied by 10 for the sake of comparison with curve (a).

## 2.5. Enzyme reusability

As one of the advantages of immobilized enzymes is the possibility to recover and reuse the enzyme, we evaluated the reusability of some of the NP-enzyme systems after consecutive cycles of AMF activation. Each cycle consisted of 30 min of reaction under a 252 Gauss AMF at the highest frequency used (829 kHz). After each cycle of reaction, we recovered the immobilized enzyme through magnetic separation and reused it for further substrate catalysis.

**Table 4**
Relative amount of secondary structures obtained by fitting of CD-UV (entry 1) and IR spectra (entries 2–4) of AMY in $D_2O$ (entries 1,2) and conjugated to iron oxide nanoparticles (entries 3, 4, and 5).

| # | CD-UV (in $D_2O$) | | β-turn (%) | | α-helix (%) | | unordered (%) | | β-sheet (%) |
|---|---|---|---|---|---|---|---|---|---|
| 1 | AMY | | 17.0 ± 0.8 | | 33.0 ± 1.6 | | 30.0 ± 1.5 | | 17.0 ± 0.8 |
| | IR (in $D_2O$) | Band position ($cm^{-1}$) | | Band position ($cm^{-1}$) | | Band position ($cm^{-1}$) | | Band position ($cm^{-1}$)* | |
| 2 | AMY** | 1663 | 18 | 1650 | 28 | 1637 | 36 | 1680/1625 | 18 |
| **3** | NP-AMY1** | 1662 | 13 | 1651 | 26 | 1636 | 43 | 1680/1621 | 18 |
| 4 | NP-AMY2** | 1663 | 12 | 1651 | 20 | 1635 | 49 | 1681/1621 | 19 |
| 5 | NP-AMY3** | 1662 | 13 | 1650 | 18 | 1635 | 42 | 1681/1621 | 27 |

* The two components for β-sheet result from transition dipole coupling [42].
** Residual RMS deviation error of the fitting: AMY) –0.004; NP–AMY1) –0.021; NP–AMY2) –0.007; NP-AMY3 – 0.018.

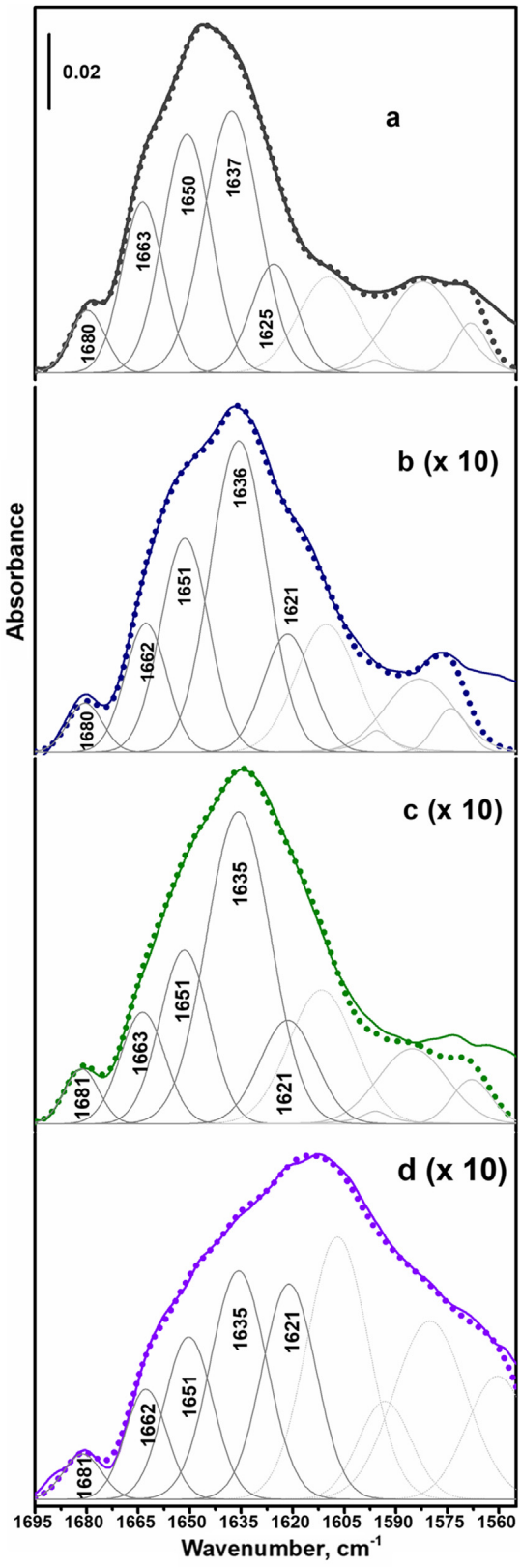


**Fig. 8.** Fitting of the amide I band of a) AMY, b) NP-AMY1, c) NP-AMY2, and d) NP-AMY3 in $D_2O$. Colored solid lines: the experimental profiles (the same as in Fig. 7); dotted colored lines: spectra resulting from the sum of the fitted components, depicted by grey lines. The component at lowest wavenumbers, depicted by light grey lines, was likely due to amino acid side chains.

In general, all the different NP-AMY systems maintained full activity for 2 cycles. After 3 cycles, NP-AMY1 and NP-AMY2 maintained the 70/80% of the starting activity, while NP-AMY3 had a significant loss of activity (Fig. 9).

NP-LASPO2 maintained all its activity for 3 cycles, while, after the same number of repeated uses, NP-LASPO3 retained only half of its original activity. Although the mechanism of energy transfer should be different from when the reaction media is heated globally, these results not only showed that it is possible to establish reuse cycles, but also reinforce the idea that enzyme orientation has to be taken into account to develop more efficient enzymatic processes under AMF activation.

## 3. Conclusions

In this work, we have conjugated two thermophilic enzymes (i.e., AMY and LASPO) to iron oxide NPs through different conjugation strategies obtaining efficient biocatalysts. We have demonstrated that these NP-enzyme systems can be successfully activated by an AMF in a "wireless" fashion. We have also shown that, notwithstanding the AMF activation, the temperature of the medium increases only slightly (Fig. 10). Indeed, non-thermophilic enzymes are able to work in the same pot with the NP-AMY systems. These results made us think that there is plenty of space among the suspended NP-enzyme systems, where a non-thermophilic enzyme can work at its optimal temperature.

Moreover, we have demonstrated the importance of the orientation of the enzyme active site respect to the NP surface. This observation encourages the search for an optimal orientation in order to implement efficient catalysis under AMF activation, as it will depend on each enzyme 3D structure and rigidity among different surface zones. Moreover, thanks to the spectroscopic studies, we have also demonstrated that the nature and the position of the chemical bound that links the enzyme to the NP can modify the 3D structure of the enzyme and that this can in turn influence the enzyme activity.

The prospects of the use of this novel approach for the selective local thermo-activation of enzymes include biomedical and biotechnological applications. As NPs could be engineered to gain access to cells through the endosomal compartment [47] or through non-endocytotic pathways [48–50] or by cell internalization techniques [51,52], the use of NP-enzyme systems to remotely control cell metabolism or for the implementation of new alternatives for enzyme/pro-drug therapy could be envisioned.

Our results also allow foreseeing a future implementation of AMF-enzyme activation for biocatalytic processes of industrial interest, as we showed it is possible to achieve a fine-tuning of the enzyme-NP interface to maximize the enzyme activation effect and its re-use. In particular, the two enzymes used are attractive for biotechnological applications. AMY is widely used in the starch industry for the conversion of starch to medium-sized oligosaccharides. LASPO can be used for the production of D-aspartate from a racemic mixture of D,L-aspartate, a molecule employed in the pharmaceutical industry, for parenteral nutrition, as a food additive and in sweetener manufacture [53]. However, the industrial application of both enzymes is hampered by the high cost per enzymatic unit, which encourage exploring the use of thermophilic enzyme to improve their reusability due to their increased stability. However, their use introduces the need to heat the reaction media to higher temperatures in order to maximize the efficiency of the reaction. As we have shown that the magnetic NPs can generate enough local amount of thermal energy for the activation of both enzymes,

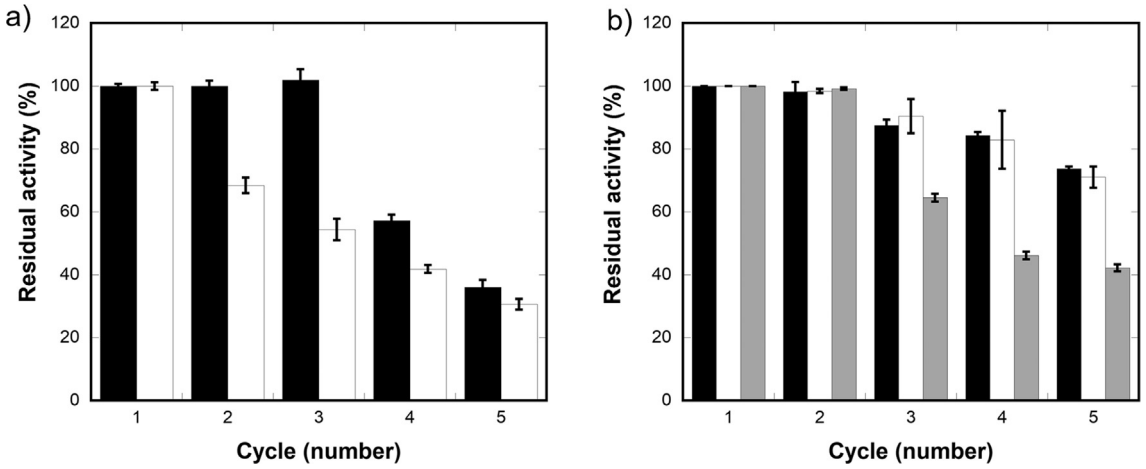


**Fig. 9.** Operational stability of NP-AMY and LASPO preparations. (a) NP-AMY1 (black), NP-AMY2 (white) and NP-AMY 3 (grey). b) NP-LASPO2 and NP-LASPO3 systems exposed to an AMF of 829 kHz and 252 Gauss.

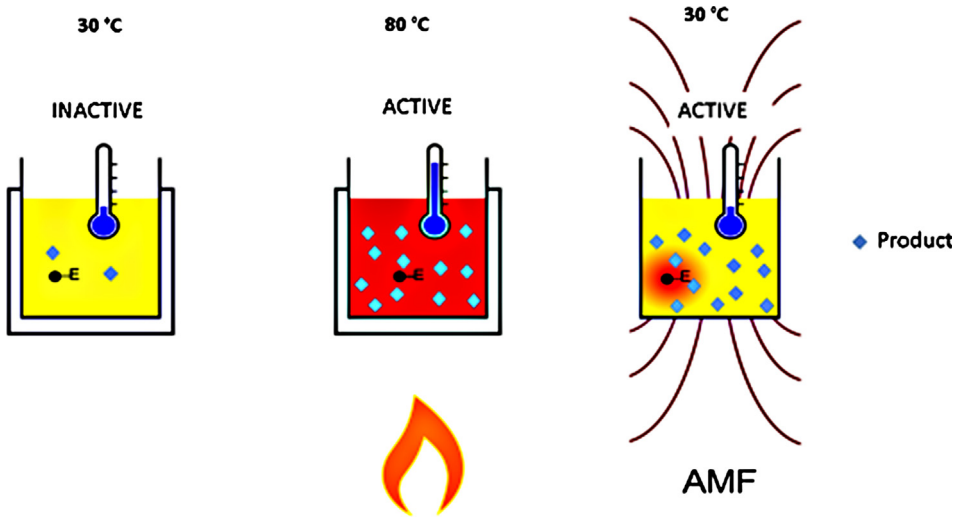


**Fig. 10.** The NP-enzyme systems (NP-AMY and NP-LASPO) are inactive at room temperature (A) and active at high temperature (B). Under an AMF of 829 kHz and 252 Gauss, the NP-enzyme systems become active as they were working in a high temperature environment.

a future implementation of AMF-enzyme activation should allow saving energy costs. Besides, as each enzyme was activated without raising the temperature of the reaction solution as a whole, the implementation of AMF-activation of multi-enzymatic processes of biotechnological interest will be also feasible.

## 4. Materials and methods

### 4.1. Chemicals

APTES, 1-ethyl-3-(3-dimethylaminopropyl) carbodiimide (EDC), Hydroxysuccinimide (NHS), 4-amino antipyrine (4-AAP), L-aspartate acid, Phenol, Orange II, Tris-HCl; Sodium tetraborate, Starch from potatoes, Potassium sodium tartrate, tetrahydrate, 3,5-Dinitrosalicylic acid, D (+) Maltose, monohydrate; all purchased from Sigma Aldrich. Horse Radish Peroxidase, EIA grade (POD) was purchased from Roche (10814407001), sulfosuccinimidyl 4-(N-maleimidomethyl)cyclohexane-1-carboxylate (sulfo-SMCC) and bis(sulfosuccinimidyl)suberate (BS3) were purchased from ThermoFisher Scientific. Amino terminated polyethylene glycol (700 Da PEG-$NH_2$) was purchased from Rapp Polymere.

### 4.2. Enzymes

AMY from *Bacillus licheniphormis* was purchased from SIGMA (25,1 mg/mL, 932 U/mg prot – A3403-500KU). LASPO used is this work is the wild type from *Sulfolobus tokodaii* that was overexpressed in *Escherichia coli* cells and purified to >95% purity as described by Bifulco et al [54]. The purified batch of LASPO (2.255 U/mL; 0.37 U/mg) was stored in 20 mM Tris–HCl buffer at pH 7.5 and 10% glycerol. D-amino acid oxidase from *Rhodotorula gracilis* (DAAO) was produced as recombinant protein in *E. coli* and purified as stated. The purified DAAO (90 U/mg) was stored in 50 mM Potassium Phosphate buffer pH 7.5, 2 mM EDTA, 10% glycerol and 5 mM 2-mercaptoethanol [55].

### 4.3. Synthesis of the iron oxide nanoparticles and functionalization with APTES

Iron oxide NPs were synthetized with a co-precipitation method according to Balzaretti et al. [22]. Briefly, 8.89 g of $FeCl_3 \times 6\ H_2O$ and 3.28 g $FeCl_2 \times 4\ H_2O$ were mixed in 380 mL of water, while slowly dropping 1.5 mL of 37%HCl into the solution

and maintained under a vigorous stirring for 30 min. Then, 25 mL of 25% $NH_4OH$ were added and stirred vigorously for 10 min. NPs were washed three times with MilliQ water and 40 mL of 2 M $HNO_3$ were added and heated at 90 °C for 5 min. Particles were separated by a magnet and 60 mL of 0.34 M solution of Fe $(NO_3)_3 \times 9\ H_2O$ were added. The suspension was heated at 90 °C for 30 min, after which the supernatant was removed and IONPs were collected by a magnet, suspended in MilliQ water and left in dialysis overnight. To 150 mg of IONPs suspended in MilliQ water was added 1 mL of a solution of 1.5 M APTES in ethanol. The reaction was maintained under mechanical stirring for 1 h at room temperature and for 1 h at 90 °C. The amino-modified NPs (NP-APTES) were washed three times with MilliQ water, separated by centrifugation and suspended in MilliQ water. The obtained NPs were stored at 4 °C.

### 4.4. L-aspartate oxidase reduction

The enzyme reduction of LASPO was exploited through the TCEP reducing gel (PIERCE) according to the manufacturer protocol. Briefly, 1 mg of enzyme was added to an equal volume of TCEP reducing gel. The sample was incubated at RT under mechanical stirring for 45 min. The enzyme was centrifuged at 1000 rpm for 30 s. The supernatant was removed and discarded. After incubation, the sample was transferred into a spincup column, previously placed in a new tube, and centrifuge at 1000 rpm for 1 min. To determine the number of reduced thiol groups, was used the Ellman's Reagent. This reagent reacts with sulfhydryl groups to produce 1 mol of 2-nitro-5-thiobenzoic acid (which absorbs at 412 nm) per mole of sulfhydryl group.

### 4.5. Enzymes conjugation

8 mg of NP-APTES were sonicated in 20 mM sodium phosphate buffer and 6,7 mM HCl at pH 7 (NP-AMY1) or at pH 9 (NP-AMY2). Then a solution of EDC an NHS, in a final concentration of respectively 39 mM and 26 mM, was added under sonication in a final volume of 2 mL. Finally, 400 μg of α-amylase were added and the reaction was carried out for 24 h at 4 °C on a rotating plate tube stirrer. Subsequently, α-amylase conjugated NPs were collected by a magnet and washed twice with 2 mL of buffer. For the conjugation of AMY through the enzyme primary amine, a BS3 solution (10 μM final concentration) was added to 1 mg of NP-APTES in 10 mM borate buffer pH 8.2. The reaction was maintained under mechanical stirring for 30 min at room temperature, then 1 mg of enzyme was added and the reaction was conducted at 40 °C for 2 h in a final volume of 1 mL. After the addition of 100 mM Tris-HCl, the particles were isolated and, after several washes, were suspended in 1 mL of 10 mM borate buffer pH 8.2. The resulting conjugated enzyme was stored at 4 °C until use. LASPO conjugation was performed with five different strategies: for the standard protocol, 16 mg of NP-APTES were sonicated in 5 mM sodium pyrophosphate buffer at pH 8.5. Then a solution of EDC (65 mM final concentration) and NHS (13 mM final concentration) were added under sonication in a final volume of 2 mL, following by the addition of 200 μg of pure LASPO. The reaction was carried for 2 h at room temperature on a rotating plate tube stirrer. Subsequently, LASPO conjugated NPs (NP-LASPO) were collected by a magnet and washed twice with 2 mL of 5 mM sodium pyrophosphate buffer, pH 8.5.

For the sulfo-SMCC- cysteine strategy, 1 mg of NP-APTES were suspended in 5 mM sodium pyrophosphate buffer pH 5, followed by the addition of a solution of sulfo-SMCC at a final concentration of 4 μM in a final volume of 1 mL. The reaction was incubated for 30 min at room temperature under mechanical stirring. After several washes, 1 mg the previously reduced enzyme was added and the reaction was maintained under mechanical stirring for 30 min at room temperature. Then the particles were isolated by a magnet and suspended, after several washes, in 5 mM sodium pyrophosphate buffer pH 5.

For the conjugation of LASPO through the enzyme primary amine, a BS3 solution (10 μM final concentration) was added to 1 mg of NP-APTES in 10 mM borate buffer pH 8.2. The reaction was maintained under mechanical stirring for 30 min at room temperature, then 1 mg of enzyme was added and the reaction was conducted at 40 °C for 2 h in a final volume of 1 mL. After the addition of 100 mM Tris-HCl, the particles were isolated and, after several washes, were suspended in 1 mL of 10 mM borate buffer pH 8.2. For the NTA functionalization method, the NTA-$Cu^{2+}$ (40 μM final concentration) was introduced onto the NP-APTES following the same procedure of the BS3 functionalization method. The reaction was carried on in a final volume of 1 mL. The particles obtained were then incubated for 1 h at room temperature in presence of 1 mg of enzyme. The resulting NP-LASPO4 were isolated and, after several washes were suspended in 1 mL of 10 mM borate buffer pH 8.2.

For the last strategy, NP-APTES were modified with 18 μM of PEG-$NH_2$ in 1 mL final volume, using the BS3 protocol. After the addition of a BS3 solution, which reacted with the PEG-NP-APTES 30 min at room temperature, 1 mg of LASPO was added and the reaction was conducted for 2 h at 40 °C. The resulting conjugated enzyme was stored at 4 °C until use.

DAAO was conjugated as previously reported [22].

For each conjugation strategy, the amount of unbound enzyme was evaluated by means of a Bradford assay, and the conjugation yield was calculated by the percentage of the ratio of the bound enzyme and the total enzyme put in the reaction.

### 4.6. Determination of amine group on the NP surface

The amino content of the NPs was measured by the Orange II spectrophotometric assay [23,24]. A total of 1 mg of NPs was mixed in 1 mL of 14 mg/mL of Orange II solution at pH 3 and maintained under stirring for 30 min at 40 °C. The particles were precipitated and washed with an acidic water solution until all the unbound dye was removed. To desorb the bound dye, a solution at pH 12 was added to the NPs. The amount of desorbed dye was then measured at a wavelength of 480 nm with a Varian Cary 50 UV/vis spectrophotometer.

### 4.7. Magnetic characterization of nanoparticles

The magnetic properties of the particles were determined with SQUID magnetometer (MPMS-XL Quantum Design). The sample was dried on a piece of cotton and was analysed with a field that vary from 50,000 Oe to −50,000 Oe at 300 K.

### 4.8. Transmission electron microscopy (TEM)

TEM bright field measurements were performed with the samples diluted in $H_2O$ MilliQ using a TECNAI G2 microscope operating at 200 kV. The software ImageJ was used for calculating the average core diameter, size distributions and standard deviations of each sample by averaging 200 NPs from TEM images.

### 4.9. Dynamic light scattering (DLS) and electrophoretic mobility (ζ-potential) analysis

Nanoparticle hydrodynamic diameter and polydispersity index (PDI) were measured in milliQ water. NPs dispersions were prepared by diluting the NP stock to the required concentration. ζ-potential measurements were performed with the samples diluted in 1 mM KCl at 25 °C. For NP-APTES, stability measurements, DLS

analysis and ζ-potential were carried out in milliQ water in a range of pH from 3 to 12 and at different NaCl concentrations. Measurements were performed at 25 °C using 90 Plus Particle Size Analyzer (Brookhaven Instrument Corporation).

### 4.10. Enzymes activity assay

The enzymatic activity of free and conjugated AMY was quantitatively assessed using a 3,5-dinitrosalicyclic acid colorimetric assay. Starch was prepared for all experiments in the buffer of desired pH and gelatinized by heating until boiling for 10 min.

The LASPO and NP-LASPO activity was assayed by measuring the initial rate of production of $H_2O_2$ with a coupled peroxidase/dye assay. The $H_2O_2$ reacts with phenol and 4-aminoantipyrine (4-AAP) by the catalytic action of peroxidase to form a red coloured quinoamine dye complex. The dye produced was detected with a spectrophotometer at 505 nm ($\varepsilon = 6.58\ mM^{-1}\ cm^{-1}$) and 25 °C. According to Bifulco et al. [54], the standard assay mixture contained: 50 mM of Sodium Pyrophosphate, 1.5 mM 4-AAP, 2 mM Phenol, 20 μM FAD (flavin adenine dinucleotide), 10 mM L-Aspartate, 2.5 U of POD (horseradish peroxidase), in a final volume of 1 mL.

### 4.11. Preparation of AMY solution in $D_2O$

The sampling used for acquire IR spectra of NP–AMY1, 2 and 3 required the suspensions in $D_2O$ (see below), thus also CD-UV spectra of AMY were collected in such solvent, for the sake of consistency. To attain this condition, the parent AMY solution in $H_2O$ was filtered in centrifuge tube with membrane (cut–off 10 kDa; centrifugation at 4000 RPM for 10 min) with 5 subsequent $D_2O$ dissolution-filtration by centrifugation cycles resulting in a final AMY-$D_2O$ 20 mg $mL^{-1}$ solution. The completeness of the $H_2O$/$D_2O$ substitution was assessed by IR spectroscopy (Fig. S6 in the Supporting Information), that also revealed the complete removal of sucrose initially present in the parent solution.

### 4.12. Circular dichroism spectroscopy (CD-UV)

For these measurements, $D_2O$ was used as a solvent for consistency with the IR ones. The spectra of 0.07 mg $mL^{-1}$ AMY solution in $D_2O$ and NP-AMY1, 2 and 3 suspensions with a similar estimated amount of AMY, were scanned in the far–UV spectral range (average of four accumulations) over the wavelength region of 180–300 nm, scanning speed of 50 nm $min^{-1}$. Spectra of NP functionalized with APTES and suspended in $D_2O$ were collected, also, for the sake of comparison. Spectra were acquired with a Jasco J-815 spectropolarimeter equipped with a Xe arc lamp and a quartz cuvette (path length 0.1 cm). Resulting CD spectra were then fitted using CDNN deconvolution software (Version 2.1, Copyright 1997 Gerald Böhm) for the secondary structure estimation. CDNN software works with a neural network, an artificial intelligence program used to find correlation with reference database spectra. Parameters such as molecular mass (in Daltons), protein concentration (in $mg{\cdot}mL^{-1}$), number of amino acids, and cuvette path length (in centimeters) were used as input to upload CD files, expressed in mdeg in the 180–260 nm range. The deconvolution was made considering the maximum number (33) of reference spectra in the database. Only results not exceeding the 100% of total sum of secondary structure and the 5% of standard deviation were considered as reliable in the 185–260 nm range.

### 4.13. Infrared spectra (IR)

Spectra were collected in the ATR mode using a Bruker IFS28 spectrometer (resolution 4 $cm^{-1}$; detector MCT). In the case of AMY aqueous solutions, a horizontal cell (by Specac, internal reflection element – IRE: ZnSe; 5 internal reflections) was used. For NP–AMY1, NP–AMY2, and NP-AMY3 the main target was to keep the samples in an aqueous environment, in order to avoid possible changes in the enzyme structure due to drying and inclusion in a KBr matrix, as in the usual sampling based on conventional pelleting. To this, samples in the form of slurry must be prepared and pressed on the IRE of an ATR cell, conversely the simple contact of the suspension with the IRE did not result in an amount of nanoparticles within the evanescent wave paths high enough to obtain any detectable absorption signal. The complete coverage of the IRE of a horizontal-ATR cell requires a significant amount of slurry. To overcome this problem, a single reflection ATR cell with IRE in diamond was used (Golden Gate cell with ZnSe lenses, by Specac). Therefore, the intensity of the absorption band was quite weak (see Fig. S7 in the Supporting Information), thus the correctness of the subtraction of the contribution due to the $\delta H_2O$ mode from the spectral pattern in the 1750–1550 $cm^{-1}$ range, resulting from the superposition of such signal and the amide I band of enzymes linked to nanoparticles become crucial. To avoid subtraction artifacts, $H_2O$ was replaced with $D_2O$, resulting in the replacement of the $\delta H_2O$ band by the $\delta D_2O$, falling at ca. 1200 $cm^{-1}$ (see Fig. S7 in the Supporting Information). Moreover, the H/D isotopic exchange resulted also in a downshift of the $\delta NH_2$ band of amino groups exposed by functionalized NP, thus no longer contributing to the spectral pattern where the amide I band falls. For pressing, a piece of $CaF_2$ was put between the slurry and the press, and this also prevented the occurrence of any significant dissolution of $H_2O$ molecules from moisture in $D_2O$ wetting the slurry. To obtain the spectra of AMY conjugated to nanoparticles, the spectrum of a slurry of NP-APTES in $D_2O$ was subtracted as a background (see Fig. S7 in the Supporting Information). All spectra resulted from the average of 250 scans. The fitting of the Amide I band of AMY was carried out by exploiting the relevant tool present in the OPUS® 5.0 Spectroscopy Sotfware, by Bruker Optik GmbH.

### 4.14. Hyperthermia analysis

For AMY, hyperthermia analyses were carried on in the frequency range of 419–829 kHz with an amplitude of 252 Gauss. For LASPO the hyperthermia analysis were performed at 829 KHz and 252 Gauss. were carried on in a final volume of 1 mL with 400 μg of NPs. The measurements were performed using D500 series (Nanoscale Biomaterial).

## Acknowledgements

Ilaria Armenia is a PhD student of the "Biotechnology, Biosciences and Surgical Technology" course at Università degli Studi dell'Insubria. The Authors are in debt with Prof. Loredano Pollegioni for the gift of the enzymes LASPO and DAAO. Authors would like to also acknowledge the public funding from Fondo Social de la DGA, Spain (grupos DGA), and from Ministerio de la Economía y Competitividad del Gobierno de España for the public funding of Proyectos I D+i – Programa Estatal de Investigación, Desarrollo e Innovación Orientada a los Retos de la Sociedad, Spain (project n. BIO2017-84246-C2-1-R). The Authors thank Dr Gianluca Tomasello for the use of 3DPROTEINIMAGING (https://3dproteinimaging.com).

## Appendix A. Supplementary material

Supplementary data to this article can be found online at https://doi.org/10.1016/j.jcis.2018.11.058.

## References


[1] O. Kirk, T.V. Borchert, C.C. Fuglsang, Industrial enzyme applications, Curr. Opin. Biotechnol. 13 (2002) 345–351, https://doi.org/10.1016/S0958-1669(02)00328-2.

[2] A. Madhavan, R. Sindhu, P. Binod, R.K. Sukumaran, A. Pandey, Strategies for design of improved biocatalysts for industrial applications, Bioresour. Technol. (2017), https://doi.org/10.1016/j.biortech.2017.05.031.

[3] I. Eş, J.D.G. Vieira, A.C. Amaral, Principles, techniques, and applications of biocatalyst immobilization for industrial application, Appl. Microbiol. Biotechnol. 99 (2015) 2065–2082, https://doi.org/10.1007/s00253-015-6390-y.

[4] H.H.P. Yiu, M.A. Keane, Enzyme-magnetic nanoparticle hybrids: new effective catalysts for the production of high value chemicals, J. Chem. Technol. Biotechnol. 87 (2012) 583–594, https://doi.org/10.1002/jctb.3735.

[5] M. Suzuki, A. Aki, T. Mizuki, T. Maekawa, R. Usami, H. Morimoto, Encouragement of enzyme reaction utilizing heat generation from ferromagnetic particles subjected to an AC magnetic field, PLoS One 10 (2015) 1–11, https://doi.org/10.1371/journal.pone.0127673.

[6] S. Datta, L.R. Christena, Y.R.S. Rajaram, Enzyme immobilization: an overview on techniques and support materials, 3 Biotech. 3 (2013) 1–9, https://doi.org/10.1007/s13205-012-0071-7.

[7] A.H. Lu, E.L. Salabas, F. Schüth, Magnetic nanoparticles: synthesis, protection, functionalization, and application, Angew. Chemie – Int. Ed. 46 (2007) 1222–1244, https://doi.org/10.1002/anie.200602866.

[8] R. Ahmad, M. Sardar, Enzyme immobilization: an overview on nanoparticles as immobilization matrix, Biochem. Anal. Biochem. 04 (2015) 1–8, https://doi.org/10.4172/2161-1009.1000178.

[9] P. Tartaj, M.P. Morales, T. González-Carreño, S. Veintemillas-Verdaguer, C.J. Serna, Advances in magnetic nanoparticles for biotechnology applications, J. Magn. Magn. Mater. 290–291 PA (2005) 28–34, https://doi.org/10.1016/j.jmmm.2004.11.155.

[10] W. Wu, Z. Wu, T. Yu, C. Jiang, W.-S. Kim, Recent progress on magnetic iron oxide nanoparticles: synthesis, surface functional strategies and biomedical applications, Sci. Technol. Adv. Mater. 16 (2015) 023501, https://doi.org/10.1088/1468-6996/16/2/023501.

[11] R. Hergt, S. Dutz, R. Müller, M. Zeisberger, Magnetic particle hyperthermia: nanoparticle magnetism and materials development for cancer therapy, J. Phys. Condens. Matter. 18 (2006) S2919–S2934, https://doi.org/10.1088/0953-8984/18/38/S26.

[12] M. Moros, A. Ambrosone, G. Stepien, F. Fabozzi, V. Marchesano, A. Castaldi, A. Tino, J. de la Fuente, C. Tortiglione, Deciphering intracellular events triggered by mild magnetic hyperthermia in vitro and in vivo, Nanomedicine (Lond.) 10 (2015) 2167–2183, https://doi.org/10.2217/nnm.15.70.

[13] A.M. Schmidt, Induction heating of novel thermoresponsive ferrofluids, J. Magn. Magn. Mater. 289 (2005) 5–8, https://doi.org/10.1016/j.jmmm.2004.11.003.

[14] T. Mizuki, M. Sawai, Y. Nagaoka, H. Morimoto, T. Maekawa, Activity of lipase and chitinase immobilized on superparamagnetic particles in a rotational magnetic field, PLoS One 8 (2013), https://doi.org/10.1016/j.bbrc.2010.02.081.

[15] T. Mizuki, N. Watanabe, Y. Nagaoka, T. Fukushima, H. Morimoto, R. Usami, T. Maekawa, Activity of an enzyme immobilized on superparamagnetic particles in a rotational magnetic field, Biochem. Biophys. Res. Commun. 393 (2010) 779–782, https://doi.org/10.1016/j.bbrc.2010.02.081.

[16] N.L. Klyachko, M. Sokolsky-Papkov, N. Pothayee, M.V. Efremova, D.A. Gulin, N. Pothayee, A.A. Kuznetsov, A.G. Majouga, J.S. Riffle, Y.I. Golovin, A.V. Kabanov, Changing the enzyme reaction rate in magnetic nanosuspensions by a non-heating magnetic field, Angew. Chem. – Int. Ed. 51 (2012) 12016–12019, https://doi.org/10.1002/anie.201205905.

[17] A. Zakharchenko, N. Guz, A.M. Laradji, E. Katz, S. Minko, Magnetic field remotely controlled selective biocatalysis, Nat. Catal. (2017) 1–9, https://doi.org/10.1038/s41929-017-0003-3.

[18] N. Kato, A. Oishi, F. Takahashi, Enzyme reaction controlled by magnetic heating due to the hysteresis loss of γ-$Fe_2O_3$ in thermosensitive polymer gels immobilized β-galactosidase, Mater. Sci. Eng. C 6 (1998) 291–296, https://doi.org/10.1016/S0928-4931(98)00065-4.

[19] F. Takahashi, Y. Sakai, Y. Mizutani, Immobilized enzyme reaction controlled by magnetic heating: γ-$Fe_2O_3$- loaded thermosensitive polymer gels consisting of N-isopropylacrylamide and acrylamide, J. Ferment. Bioeng. 83 (1997) 152–156, https://doi.org/10.1016/S0922-338X(97)83574-X.

[20] M. Suzuki, H. Hayashi, T. Mizuki, T. Maekawa, H. Morimoto, Efficient DNA ligation by selective heating of DNA ligase with a radio frequency alternating magnetic field, Biochem. Biophys. Reports. 8 (2016) 360–364, https://doi.org/10.1016/j.bbrep.2016.10.006.

[21] A.K. Gupta, M. Gupta, Synthesis and surface engineering of iron oxide nanoparticles for biomedical applications, Biomaterials 26 (2005) 3995–4021, https://doi.org/10.1016/j.biomaterials.2004.10.012.

[22] R. Balzaretti, F. Meder, M.P. Monopoli, L. Boselli, I. Armenia, L. Pollegioni, G. Bernardini, R. Gornati, Synthesis, characterization and programmable toxicity of iron oxide nanoparticles conjugated with D-amino acid oxidase, RSC Adv. (2017).

[23] S. Noel, B. Liberelle, L. Robitaille, G. De Crescenzo, Quantification of primary amine groups available for subsequent biofunctionalization of polymer surfaces, Bioconjug. Chem. 22 (2011) 1690–1699, https://doi.org/10.1021/bc200259c.

[24] R. Arenal, L. De Matteis, L. Custardoy, A. Mayoral, M. Tence, V. Grazu, J.M. De La Fuente, C. Marquina, M.R. Ibarra, Spatially-resolved EELS analysis of antibody distribution on biofunctionalized magnetic nanoparticles, ACS Nano 7 (2013) 4006–4013, https://doi.org/10.1021/nn306028t.

[25] Y. Liu, Y. Li, X.M. Li, T. He, Kinetics of (3-aminopropyl)triethoxylsilane (aptes) silanization of superparamagnetic iron oxide nanoparticles, Langmuir 29 (2013) 15275–15282, https://doi.org/10.1021/la403269u.

[26] D. Dorniani, M.Z. Bin Hussein, A.U. Kura, S. Fakurazi, A.H. Shaari, Z. Ahmad, Sustained release of prindopril erbumine from its chitosan-coated magnetic nanoparticles for biomedical applications, Int. J. Mol. Sci. 14 (2013) 23639–23653, https://doi.org/10.3390/ijms141223639.

[27] M. Mahmoudi, S. Sant, B. Wang, S. Laurent, T. Sen, Superparamagnetic iron oxide nanoparticles (SPIONs): development, surface modification and applications in chemotherapy, Adv. Drug Deliv. Rev. 63 (2011) 24–46, https://doi.org/10.1016/j.addr.2010.05.006.

[28] C. Wang, K. Zhang, Z. Zhou, Q. Li, L. Shao, R.Z. Hao, X. Rui, S. Wang1, Vancomycin-modified $Fe_3O_4$ @$SiO_2$ @Ag microflowers as effective antimicrobial agents, Int. J. Nanomed. 12 (2017) 3077–3094, https://doi.org/10.1039/c0cc05390b.

[29] M. Chen, G. Zeng, P. Xu, C. Lai, L. Tang, How do enzymes 'meet' nanoparticles and nanomaterials?, Trends Biochem Sci. (2017) 1–17, https://doi.org/10.1016/j.tibs.2017.08.008.

[30] F. Secundo, Conformational changes of enzymes upon immobilisation, Chem. Soc. Rev. 42 (2013) 6250, https://doi.org/10.1039/c3cs35495d.

[31] A. Sassolas, L.J. Blum, B.D. Leca-Bouvier, Immobilization strategies to develop enzymatic biosensors, Biotechnol. Adv. 30 (2012) 489–511, https://doi.org/10.1016/j.biotechadv.2011.09.003.

[32] S. Knecht, D. Ricklin, A.N. Eberle, B. Ernst, Oligohis-tags: mechanisms of binding to Ni2+-NTA surfaces, J. Mol. Recognit. 22 (2009) 270–279, https://doi.org/10.1002/jmr.941.

[33] Y. Nozaki, C. Tanford, Examination of titration behavior, in: Methods Enzymol., Academic Press, 1967, pp. 715–734, https://doi.org/10.1016/S0076-6879(67)11088-4.

[34] M. Moros, B. Hernàez, E. Garet, J.T. Dias, B. Saez, V. Grazu, A. Gonzales-Fernandez, C. Alfonso, J.M. de la Fuente, Monosaccharides versus PEG-functionalized NPs: influence in the cellular uptake, ACS Nano 6 (2012) 1565–1577.

[35] B. Pelaz, P. Del Pino, P. Maffre, R. Hartmann, M. Gallego, S. Rivera-Fernandez, J.M. de la Fuente, G.U. Nienhaus, W.J. Parak, Surface functionalization of nanoparticles with polyethylene glycol: effects on protein adsorption and cellular uptake, ACS Nano 9 (2015) 6996–7008, https://doi.org/10.1021/acsnano.5b01326.

[36] S. Puertas, P. Batalla, M. Moros, E. Polo, P. Del Pino, J.M. Guisàn, V. Grazù, J.M. de la Fuente, Taking advantage of unspecific interactions to produce highly active magnetic nanoparticles – antibody conjugates, ACS Nano 5 (2011) 4521–4528.

[37] I. Armenia, R. Balzaretti, C. Pirrone, C. Allegretti, P. D'Arrigo, M. Valentino, R. Gornati, G. Bernardini, L. Pollegioni, L -Aspartate oxidase magnetic nanoparticles: synthesis, Characterization and L -Aspartate Bioconversion, RSC Adv. 7 (2017) 21136–21143, https://doi.org/10.1039/C7RA00384F.

[38] M. Jain, A. Mariya Sebatini, P. Radha, S. Kiruthika, C. Muthukumaran, K. Tamilarasan, Synthesis, characterization and kinetic analysis of chitosan coated magnetic nanobiocatalyst and its application on glucose oleate ester synthesis, J. Mol. Catal. B Enzym. 128 (2016) 1–9, https://doi.org/10.1016/j.molcatb.2016.02.006.

[39] J. Xu, J. Sun, Y. Wang, J. Sheng, F. Wang, M. Sun, Application of iron magnetic nanoparticles in protein immobilization, Molecules 19 (2014) 11465–11486, https://doi.org/10.3390/molecules190811465.

[40] C. Wang, C.H. Hsu, Z. Li, L.P. Hwang, Y.C. Lin, P.T. Chou, Y.Y. Lin, Effective heating of magnetic nanoparticle aggregates for in vivo nano-theranostic hyperthermia, Int. J. Nanomed. 12 (2017) 6273–6287, https://doi.org/10.2147/IJN.S141072.

[41] H. Fabian, W. Mäntele, Infrared Spectroscopy of Proteins, Wiley, Chichester, 2006.

[42] H. Fabian, W. Mäntele, Infrared Spectroscopy of proteins, in: J.M. Chalmers, P. R. Griffiths (Eds.), Handb. Vib. Spectrosc, Wiley, Chichester, 2002, pp. 3399–3425.

[43] Y.Y. Su, B. Jirgensons, Further studies of detergent-induced conformational transitions in proteins. Circular dichroism of ovalbumin, bacterial alpha-amylase, papain, and beta-lactoglobulin at various pH values, Arch. Biochem. Biophys. 181 (1977) 137–146, https://doi.org/10.1016/0003-9861(77)90491-X.

[44] B.A. Kikani, S.P. Singh, Enzyme stability, thermodynamics and secondary structures of α-amylase as probed by the CD spectroscopy, Int. J. Biol. Macromol. 81 (2015) 450–460, https://doi.org/10.1016/j.ijbiomac.2015.08.032.

[45] J. Fitter, J. Heberle, Structural equilibrium fluctuations in mesophilic and thermophilic α-amylase, Biophys. J. 79 (2000) 1629–1636, https://doi.org/10.1016/S0006-3495(00)76413-7.

[46] K. Berthelot, F. Immel, J. Géan, S. Lecomte, R. Oda, B. Kauffmann, C. Cullin, Driving amyloid toxicity in a yeast model by structural changes: a molecular approach, FASEB J. 23 (2009) 2254–2263, https://doi.org/10.1096/fj.08-125724.

[47] E. Papis, F. Rossi, M. Raspanti, I. Dalle-Donne, G. Colombo, A. Milzani, G. Bernardini, R. Gornati, Engineered cobalt oxide nanoparticles readily enter cells, Toxicol. Lett. 189 (2009) 253–259, https://doi.org/10.1016/j.toxlet.2009.06.851.

[48] D. Zanella, E. Bossi, R. Gornati, C. Bastos, N. Faria, G. Bernardini, Iron oxide nanoparticles can cross plasma membranes, Sci. Rep. 7 (2017) 11413, https://doi.org/10.1038/s41598-017-11535-z.
[49] E. Bossi, D. Zanella, R. Gornati, G. Bernardini, Cobalt oxide nanoparticles can enter inside the cells by crossing plasma membranes, Sci. Rep. 6 (2016) 22254, https://doi.org/10.1038/srep22254.
[50] H. Zhang, Q. Ji, C. Huang, S. Zhang, B. Yuan, K. Yang, Y. Ma, Cooperative transmembrane penetration of nanoparticles, Sci. Rep. 5 (2015) 10525, https://doi.org/10.1038/srep10525.
[51] E. Zhang, M.F. Kircher, M. Koch, L. Eliasson, S.N. Goldberg, E. Renström, Dynamic magnetic fields remote-control apoptosis via nanoparticle rotation, ACS Nano 8 (2014) 3192–3201, https://doi.org/10.1021/nn406302j.
[52] Y. Kaizuka, T. Ura, S. Lyu, L. Chao, J. Henzie, H. Nakao, Cytosolic transport of nanoparticles through pressurized plasma membranes for molecular delivery and amplification of intracellular fluorescence, Langmuir 32 (2016) 13534–13545, https://doi.org/10.1021/acs.langmuir.6b03412.
[53] L. Pollegioni, P. Motta, G. Molla, L-Amino acid oxidase as biocatalyst: a dream too far?, Appl Microbiol. Biotechnol. 97 (2013) 9323–9341, https://doi.org/10.1007/s00253-013-5230-1.
[54] D. Bifulco, L. Pollegioni, D. Tessaro, S. Servi, G. Molla, A thermostable L-aspartate oxidase: a new tool for biotechnological applications, Appl. Microbiol. Biotechnol. 97 (2013) 7285–7295, https://doi.org/10.1007/s00253-013-4688-1.
[55] S. Fantinato, L. Pollegioni, P. Mirella, Engineering, expression and purification of a His-tagged chimeric D-amino acid oxidase from Rhodotorula gracilis, Enzyme Microb. Technol. 29 (2001) 407–412, https://doi.org/10.1016/S0141-0229(01)00400-8.